Research Article Vol. 2, No. 2 / February 2015 / Optica 70

Efficient fiber-optical interface for nanophotonic devices

T. G. Tiecke,[1,2,†] K. P. Nayak,[1,3,†] J. D. Thompson,[1,†] T. Peyronel,[1] N. P. de Leon,[1,4] V. Vuletić,[2] and M. D. Lukin[1,*]

[1]Department of Physics, Harvard University, Cambridge, Massachusetts 02138, USA

[2]Department of Physics and Research Laboratory of Electronics, Massachusetts Institute of Technology, Cambridge, Massachusetts 02139, USA

[3]Center for Photonic Innovations, The University of Electro-Communications, 1-5-1 Chofugaoka, Chofu, Japan

[4]Department of Chemistry and Chemical Biology, Harvard University, Cambridge, Massachusetts 02138, USA

*Corresponding author: lukin@physics.harvard.edu

Received 29 July 2014; revised 8 December 2014; accepted 12 December 2014 (Doc. ID 218868); published 21 January 2015

We demonstrate a method for efficient coupling of guided light from a single-mode optical fiber to nanophotonic devices. Our approach makes use of single-sided conical tapered optical fibers that are evanescently coupled over the last ~10 μm to a nanophotonic waveguide. By means of adiabatic mode transfer using a properly chosen taper, single-mode fiber-waveguide coupling efficiencies as high as 97 (1)% are achieved. Efficient coupling is obtained for a wide range of device geometries, which are either singly clamped on a chip or attached to the fiber, demonstrating a promising approach for integrated nanophotonic circuits, and quantum optical and nanoscale sensing applications.

OCIS codes: (230.7370) Waveguides; (060.4005) Microstructured fibers; (220.4241) Nanostructure fabrication; (350.4238) Nanophotonics and photonic crystals.

http://dx.doi.org/10.1364/OPTICA.2.000070

1. INTRODUCTION

The field of nanophotonics [1] opened new avenues for applications such as nanophotonic integrated circuits [2,3], sensing [4–7], and scalable quantum information processing [8–10]. Moreover, subwavelength confinement of optical fields enabled strong light–matter interaction at the single quantum level [11,12]. A major challenge in the field is to efficiently integrate the nanophotonic devices with conventional optical fiber networks. This challenge is due to a large mismatch between the size of the fundamental mode of the optical fiber and that of the optical modes of nanophotonic devices. This mismatch has to be bridged in order to achieve efficient coupling. Highly efficient coupling is crucial for applications such as quantum repeaters [13] or quantum networks [8] since the performance of these systems, in the limit of many nodes, deteriorates near-exponentially with photon loss between individual nodes. Additionally, highly efficient coupling enables distribution of nonclassical states of light, which are extremely fragile to photon loss.

A wide range of coupling techniques are currently being explored, including grating coupling [2] and end-firing from macroscopic fibers [14], where coupling efficiencies up to 70%–80% to on-chip waveguides have been achieved. More recently, on-chip photonic waveguides have been coupled to the waist of a biconical fiber taper [15] with an efficiency as high as 95%.

In this paper, we demonstrate a novel method to efficiently couple a single-mode fiber to a dielectric nanophotonic waveguide using a conical tapered fiber tip. The coupling is based on an adiabatic transfer of the fundamental mode of the optical fiber to the fundamental mode of the nanophotonic waveguide. Our method can be applied to general dielectric one-dimensional waveguides. In contrast to biconical tapered fibers [15], our devices are single-sided, thereby offering alternative geometries such as mechanical support for nanophotonic devices [12,16] and multiple interfaces to a single photonic chip. Additionally, compared to biconical tapered fibers, the subwavelength part of the coupler is only a few micrometers

long and is therefore less sensitive to contamination and mechanical deformations. These features open the door for new applications for interfacing to nanophotonic structures.

2. ADIABATIC COUPLING

Adiabatic mode transformation is widely used to obtain efficient power transfer through nonuniform optical waveguides [17]. The key idea is to change the waveguide cross section slowly along the propagation direction of the light such that all the optical power remains in a single eigenmode of the composite waveguide, while the coupling to other modes is suppressed. More specifically, two eigenmodes ν and μ with respective effective indices n_ν and n_μ define a characteristic beating length scale between the modes given by $z_b = \lambda/(n_\nu - n_\mu)$, where λ is the wavelength in vacuum. In order to achieve adiabatic transfer the characteristic length scale z_t over which the waveguide changes has to be large compared to z_b [18]. While the exact coupling strength depends on the details of the spatial mode profiles, we design our devices according to this intuitive length-scale argument and use numerical simulations to verify the design. A crucial feature of adiabatic mode coupling is that it is insensitive to the exact coupling strength and therefore also to the precise shape of the fiber and waveguide.

Figure 1(a) shows a schematic of a typical device. A fiber is tapered down to a conical tip, and an inversely tapered silicon nitride (Si_3N_4) waveguide is attached over 7.5 μm. In what follows, we separate the fiber tips in two regions (see Fig. 1(a)): the adiabatic fiber-waveguide coupler (I) and the tapered fiber (II), separated by plane P at the start of the waveguide. In both regions we design our devices according to the adiabaticity criterion by ensuring $z_t > z_b$. In region I the optical modes of the fiber and waveguide are coupled through their evanescent fields and form a set of hybridized supermodes. z_b is determined by the difference between the effective indices of the fundamental supermode and the higher-order supermode with the closest propagation constant (in this case radiation mode), while z_t is limited by the length of the coupling region. In region II the fiber is tapered down from a standard single-mode fiber, adiabatically transforming the core-guided HE11 mode to a cladding-guided HE11 mode. We ensure that the local taper angle $\Omega(z) \equiv \rho(z)/z_t \ll \rho(z)/z_b$, where $\rho(z)$ is the fiber radius at position z along the taper. In region II z_b is determined by the coupling of the fundamental fiber mode to the nearest higher-order mode. We follow the conventional design for biconical adiabatic fiber tapers where recently transmission efficiencies as high as 99.95% [19] have been achieved (see also [18,20] for details).

For a tapered nanophotonic waveguide that vanishes at plane P (such as that shown in Fig. 1) the cross section of refractive index profile changes smoothly along the complete coupler. For such waveguides the criteria given above are sufficient to design the coupler. However, for a waveguide with a nonvanishing cross section at P (such as the rectangular waveguide shown in Fig. 1(d)), the refractive index cross section changes discontinuously. We approximate the power transfer through P by projecting the fundamental fiber mode on the fundamental supermode at P. In order to achieve efficient power transfer, we design the coupler such that this projection is close to unity. In this case the effect of the waveguide is only a small perturbation of the fundamental fiber mode at plane P, thus enabling us to design couplers based on simple eigenmode calculations.

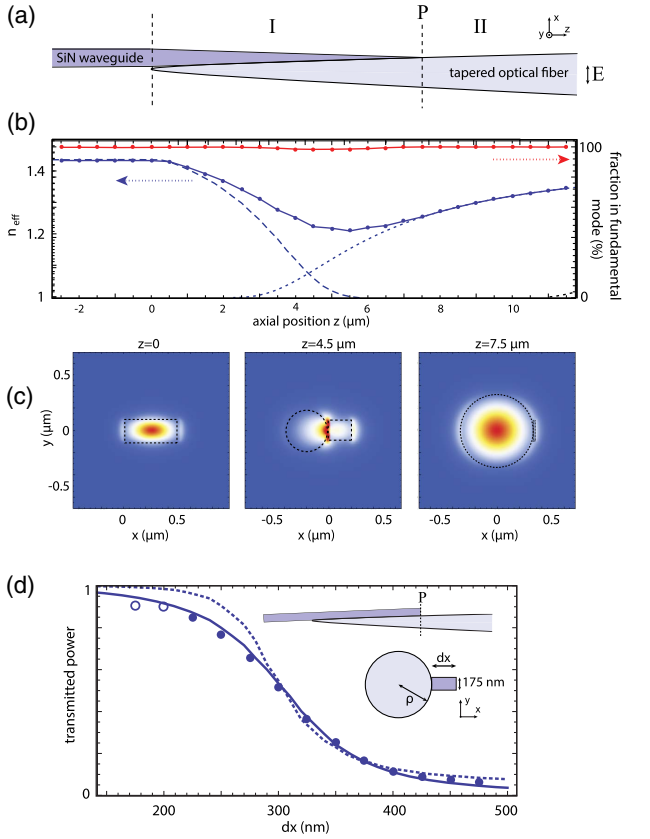

Fig. 1. Adiabatic transfer between fiber and waveguide modes. (a) Schematic of fiber-waveguide coupling. The fiber (right) has a conical shape and is attached to a tapered Si_3N_4 rectangular waveguide (left), and we consider modes polarized along $\hat{x}$. (b) Effective index n_{eff} of the fiber and waveguide modes for an opening angle of the fiber (waveguide) of 5° (4°). The blue dotted (dashed) lines are the separate fiber (waveguide) modes, and the blue solid line corresponds to the fundamental supermode of the combined structure. The red line shows the power in the fundamental supermode obtained from an FDTD simulation of the coupler (see text). (c) Cross sections of $|E|^2$ obtained from the FDTD simulation at various points along the coupler. (d) Fraction of the power in the fundamental supermode of the combined structure as a function of the waveguide width dx, obtained from a mode decomposition (solid line). The transmission through a tapered coupler (see *inset*) obtained with an FDTD simulation (circles) agrees well with the estimated transmission obtained from the mode decomposition. The two data points for $dx \leq 200$ nm (open circles) are calculated using a shallower fiber angle (2°) to ensure $z_t > z_b$. The dotted line shows the same geometry except that the fiber and waveguide are in contact on the xz plane instead of the yz plane. The fiber-waveguide cross sections used for this simulation are shown in the *inset*, $\rho = 450$ nm.

We next verify these design criteria using finite difference time domain (FDTD) simulations. Figures 1(b) and 1(c) show simulations for the device presented in Fig. 1(a). We consider a conical fiber with an opening angle $d(2\rho)/dz = 5°$ and a

$dy = 175$ nm thick Si_3N_4 waveguide with a taper angle $d(dx)/dz = 4°$ to a width of $dx = 500$ nm. We focus on TE-polarized ($\hat{x}$) modes, but we have verified that the same reasoning can be applied for TM-polarized modes. Figure 1(b) shows the effective indices of the fiber mode, the waveguide mode, and the hybridized mode of the combined structure (supermode). For this geometry, the latter has an effective index of $n_{\text{eff}} > 1.2$ over the entire length of the coupler. The combined structure supports only one other mode, which, however, has orthogonal polarization and therefore does not couple to the fundamental supermode. The relevant beat length is therefore set by the fundamental supermode and the free-space modes ($n_0 = 1$), and corresponds to $z_b \simeq 4$ μm. We chose the length of the coupler ($z_t \simeq 7$ μm) to be longer than z_b. In order to verify adiabaticity we perform a FDTD simulation (see Figs. 1(b) and 1(c)), in which we excite the fiber taper at $z = 11$ μm with the fundamental HE11 mode polarized along $\hat{x}$ and propagating along $-\hat{z}$. Along the coupler we decompose the optical fields in the basis of local eigenmodes of the combined fiber-waveguide structure and find that essentially all the optical power (>99%) is in the fundamental mode across the complete fiber-waveguide coupler, thereby confirming the adiabaticity of the coupler. As can be seen in Fig. 1(c), halfway along the coupler a large fraction of the optical power is concentrated at the interface between the fiber and the waveguide, suggesting sensitivity to scattering losses arising from surface roughness. However, we expect these effects to be negligible since the coupler length is only a few micrometers long and our fabrication methods (see Section 3) do not introduce significant surface roughness.

In the case of a rectangular waveguide (Fig. 1(d)), we model the sudden onset of the waveguide by decomposing the fundamental fiber mode in the basis of supermodes of the combined structure. This decomposition is performed using the fields of the eigenmodes of the fiber and the combined structure, which we obtain using the MIT Photonic Bands (MPB) mode-solver [21]. To verify that the projection indeed describes the power transfer accurately we compare the mode decomposition results with FDTD simulations. Figure 1(d) shows the power in the fundamental supermode of the combined structure as obtained from the mode decomposition and from an FDTD simulation for a rectangular Si_3N_4 waveguide with varying width dx and a fiber with radius $\rho = 450$ nm. We find that the loss of transmission through the coupler obtained from the FDTD simulation is well described by the mode decomposition. For the simulated conditions the losses can be made small for waveguide dimensions below 200 nm.

3. DESIGN AND FABRICATION

We next discuss the optimization and characterization of the tapered fiber tips in region II. For our experiments we use single-mode fiber (Thorlabs 780HP), with a 4.4 μm (125 μm) core (cladding) diameter, and we optimize our design for a wavelength of $\lambda = 780$ nm. Figure 2(a) shows the critical angle ($\Omega_c(z) = \rho(z)/z_b(z)$) for this fiber. In a cylindrically symmetric geometry, modes with different angular momentum do not couple; therefore, the coupling occurs between the HE11 and HE12 modes. At large fiber diameters ($d > 50$ μm) the adiabaticity criterion is determined by coupling of the HE11 core-guided mode and the cladding-guided modes, while for $d < 50$ μm the adiabaticity criterion is determined by the coupling of the HE11 and HE12 cladding-guided modes. In the latter region the critical angle scales approximately as $\Omega_c \sim \lambda/(n_{cl}\rho)$, with λ the design wavelength and n_{cl} the index of refraction of the fiber cladding. Although the design is optimized for a specific wavelength, adiabatic coupling is insensitive to the precise wavelength and therefore the coupler itself is broadband in nature.

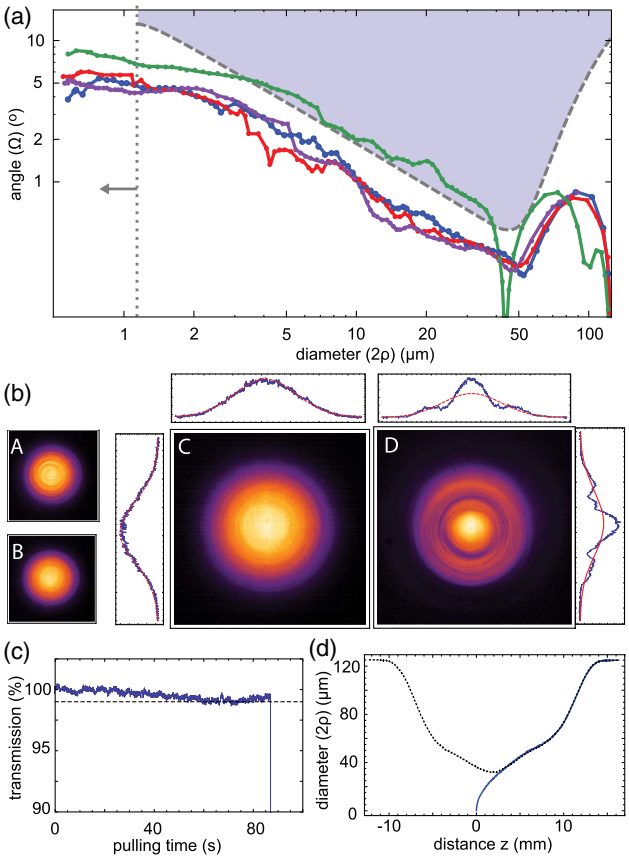

Fig. 2. Characterization of adiabatic tapers. (a) Fiber angle as a function of the local fiber diameter along the taper axis z. The dashed line and shaded area indicate the adiabaticity criterion $z_t > z_b$ as discussed in the text. Fiber tapers that have a profile below the dotted line are expected to be adiabatic. For a diameter smaller than 1.1 μm the HE12 mode is cut off. The taper profiles for four tapers [blue (A), red (B), purple (C), and green (D)] are shown. (b) Far-field mode profiles. Tapers A, B, and C show Gaussian profiles, while taper D has clear contributions from higher-order modes. For tapers C and D cuts through the center of the profiles are shown together with a Gaussian fit. (c) Transmission versus pulling time of a taper similar to A–C; the dashed line indicates 99% transmission. The sudden drop in transmission at ≃87 s arises from the fast pull by the electromagnetic coil. (d) Taper profile of taper C (blue) and of a biconical taper (dashed) using the same pulling parameters but without pulsing the electromagnet to create the tip.

We fabricate fiber tapers using a conventional heat-and-pull setup [22,23] in which the fiber is heated using an isobutane torch (140 mL/ min flow), with an effective flame length of

$L = 4.3$ mm. The flame is continuously brushed back and forth to heat the fiber over a variable length, which is adjusted during the pulling to obtain the desired fiber profile (see Refs. [22,24]). This results in a 24 mm long biconical fiber taper with a minimum diameter of ~30 μm. At this stage we apply a fast pull to one of the stages holding the fiber, which quickly (~10 ms) pulls the fiber out of the flame, thereby creating a 14 mm long fiber taper with a conical tip (see Fig. 2(d)). The fast pull is generated by an electromagnet, composed of a hard-drive head with its arm connected to one of the two fiber clamps. The clamp itself is mounted on a linear ball-bearing translation stage, and a current pulse through the electromagnet results in a constant acceleration of the fiber, creating a smooth fiber tip, which is well described by a parabolic shape at larger fiber diameters and a constant opening angle over the last tens of micrometers. We find that the acceleration changes linearly with the applied current over a range of 17 to 46 m/s^2 and we typically use an acceleration of 33 m/s^2. By optimizing the heat-and-pull-parameters we realize the requirements of the taper angle for large diameters, while the electromagnet current and fiber diameter at which the pulse is applied controls the fiber taper angle at smaller diameter. We note that the resulting parabolic shape of the fiber taper conveniently has the same scaling ($\Omega \sim 1/\rho$) as the adiabaticity criterion at the relevant range of fiber diameters (2–50 μm; see Fig. 2(a)). Additionally, our fiber tips have subwavelength dimensions only over ~10 μm and the time the fiber has a subwavelength diameter and is in the flame takes up to a few tens of milliseconds. Therefore, the requirements on the cleanliness of the flame and the fabrication environment are less stringent as compared to those for creating efficient biconical tapered fibers [19,23].

4. CHARACTERIZATION

We characterize our devices with several measurements. First, we measure the taper profiles to ensure the local angle is smaller than the critical angle set by the adiabaticity condition. Figure 2 shows three fibers (A, B, and C) that are made under the same conditions, while fiber D is made using different pulling parameters for the purpose of illustrating the performance of a suboptimal fiber taper. In Fig. 2(a) we show the fiber profiles for each fiber, which are measured using optical and scanning electron microscopy (SEM). Fibers A, B, and C show nearly identical profiles that satisfy the adiabaticity criterion, indicating that our fabrication method yields reproducible fiber tapers. Fiber D has a somewhat steeper angle for fiber diameters around ~3–30 μm and is therefore expected to be nonadiabatic. Second, in Fig. 2(b) we show the far-field profiles of the fiber mode imaged directly on a CMOS camera. The optical modes of fibers A, B, and C are all nearly Gaussian, indicating that at the end of the taper, most of the power is in the fundamental HE11 mode. Fiber D shows clearly a multimode structure, in agreement with our expectation that this taper does not match the adiabaticity criterion. To quantify the single-mode character of the profiles we calculate the coefficient of determination (R^2) of the Gaussian fits, resulting in $R^2 = 0.98, 0.99, 0.99, 0.87$ for tapers A, B, C, and D, respectively. We find this method of measuring the far-field profiles to be very fast, sensitive, and reliable for verifying the single-mode character of our fiber tips. Third, in Fig. 2(c) we show the total transmission during the time of the pulling process. We observe >99% transmission during the complete pulling process, consistent with the full biconical fiber taper being single-mode before the fast pull occurs.

After confirming that our fiber tips are single mode, we measure the coupling efficiency (η_c) to a tapered Si_3N_4 waveguide [12,16]. The waveguide we use has a photonic crystal cavity, which, away from the cavity resonance, reflects all the incident light. We measure the reflected power P_r, normalized to the power P_{in} in the fiber before the taper is pulled (see Fig. 3(a)). The normalized reflection is given by $P_r/P_{in} = \eta_c^2 \eta_m \eta_{bs} \eta_{FC}$, where η_{bs} and η_{FC} are the fiber beamsplitter and FC–FC coupling efficiencies and η_m is the Bragg mirror reflectivity (see SI). We obtain a coupling efficiency of $\eta_c = 0.97(1)$, where the error bars reflect drifts of the input power and calibrations over the course of our measurements. In comparison we achieve coupling efficiencies of $\eta_c \simeq 0.5$–0.6 for

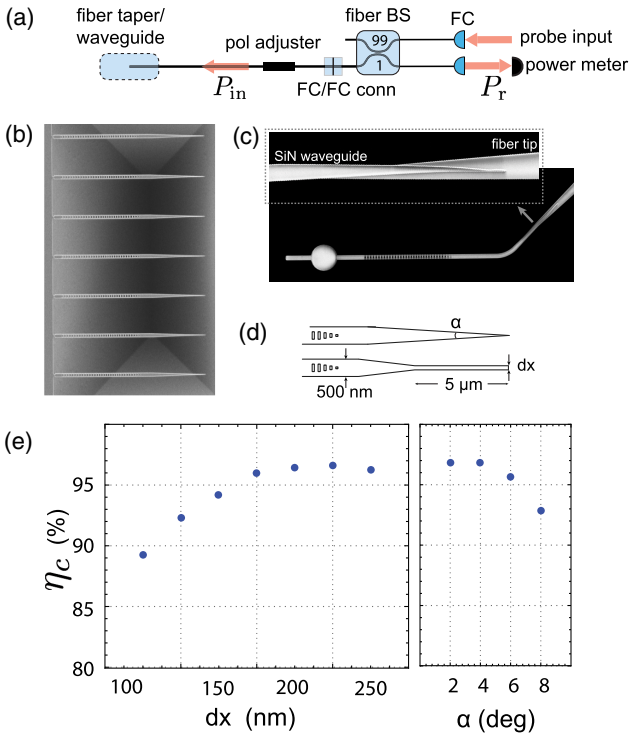

Fig. 3. Coupling to photonic crystal waveguide cavities. (a) Setup to measure fiber-waveguide coupling efficiency. A tunable probe laser is coupled weakly to the fiber connecting to the device using a 99:1 fiber beamsplitter. The polarization at the waveguide is adjusted by means of a fiber polarization controller, and the light is in and out coupled of the fiber network using fiber collimators (FCs). (b) SEM image of an array of singly clamped photonic crystal waveguide cavities used for on-chip measurements. (c) SEM image of a photonic crystal cavity attached to the fiber tip; *inset* shows a zoom of the fiber-waveguide coupler. (d) Schematic of the various waveguide geometries. (e) Coupling efficiencies for a range of waveguides; the devices are either a tapered waveguide with an opening angle α or rectangular waveguides with a varying width dx and 5 μm long before adiabatically expanding to the photonic crystal cavity. All waveguides are 175 nm thick and attached to the chip as in panel b.

fiber tips with parameters such as fiber D. Figure 3(d) shows measurements of the coupling efficiency for waveguide angles of $2° \leq \alpha \leq 8°$ and for rectangular waveguides with a width ranging from $100 < dx < 250$ nm; all waveguides have a $dy = 175$ nm thickness. For these measurements the waveguides are attached to the chip on one side only (see Fig. 3(b)). We observe that the coupling efficiency for most of these devices is ≥95%. The coupling efficiencies for $dx \leq 150$ nm are slightly lower, consistent with a not fully adiabatic coupler ($z_b > z_t$) since for decreasing waveguide width z_b increases while in our measurement we keep z_t constant.

We also detach cavities from the chip and attach them to the fiber such that they are solely connected to the fiber tip (see SI). A typical device attached in free space is shown in Fig. 3(c), for which we measure a coupling efficiency of $\eta_c = 0.96(1)$. We find that our alignment procedure (see SI) allows us to optimize the coupling efficiency in a reliable and reproducible manner; however, since we perform the alignment under an optical microscope we do not have exact knowledge of the fiber-waveguide interface. From our simulations we find that for a range of configurations the coupling efficiency is close to unity and consistent with the design criteria defined above.

5. OUTLOOK

We have presented a method for highly efficient fiber coupling to nanophotonic waveguides. Our measurements indicate coupling efficiencies as high as 97(1)% for a range of devices. These results open the door for a range of unique applications in quantum optics and nanophotonics. In particular, in combination with our recent results demonstrating strong coupling of a single atom to photonic crystals [12,16], efficient coupling to fibers can enable the creation of highly nonclassical Schrödinger cat states of light [25] and the realization of efficient protocols for scalable quantum networks [8]. Moreover, the flexible geometries as well as the fiber-based mechanical support for nanophotonic devices allowed by this approach open the door for new applications in nanoscale biosensing [6,7,26].

FUNDING INFORMATION

Air Force Office of Scientific Research (AFOSR) (RC413-G4); National Science Foundation (NSF) (Phy-0969816, Phy-1125846).

ACKNOWLEDGMENT

Financial support was provided by the NSF, the Center for Ultracold Atoms, the Natural Sciences and Engineering Research Council of Canada, the Air Force Office of Scientific Research Multidisciplinary University Research Initiative and the Packard Foundation. KPN acknowledges support from Strategic Innovation Program of Japan Science and Technology Agency (JST). JDT acknowledges support from the Fannie and John Hertz Foundation and the NSF Graduate Research Fellowship Program. This work was performed in part at the Center for Nanoscale Systems (CNS), a member of the National Nanotechnology Infrastructure Network (NNIN), which is supported by the National Science Foundation under NSF award no. ECS-0335765. CNS is part of Harvard University.

†These authors contributed equally to this work.

See Supplement 1 for supporting content.

REFERENCES

1. J. D. J. Joannopoulos, S. G. Johnson, J. N. Winn, and R. D. Meade, *Photonic Crystals: Molding the Flow of Light* (Princeton University, 2008).
2. X. Chen, C. Li, and H. K. Tsang, "Device engineering for silicon photonics," NPG Asia Mater. **3**, 34–40 (2011).
3. D. A. B. Miller, "Are optical transistors the logical next step?" Nat. Photonics **4**, 3–5 (2010).
4. D. W. Pohl, W. Denk, and M. Lanz, "Optical stethoscopy: image recording with resolution lambda/20," Appl. Phys. Lett. **44**, 651–653 (1984).
5. A. Lewis, M. Isaacson, A. Harootunian, and A. Muray, "Development of a 500 aspatial resolution light microscope: I. Light is efficiently transmitted through lambda/16 diameter apertures," Ultramicroscopy **13**, 227–231 (1984).
6. W. Tan, Z. Shi, S. Smith, D. Birnbaum, and R. Kopelman, "Submicrometer intracellular chemical optical fiber sensors," Science **258**, 778–781 (1992).
7. R. Yan, J.-H. Park, Y. Choi, C.-J. Heo, S.-M. Yang, L. P. Lee, and P. Yang, "Nanowire-based single-cell endoscopy," Nat. Nanotechnol. **7**, 191–196 (2012).
8. H. J. Kimble, "The quantum internet," Nature **453**, 1023–1030 (2008).
9. T. D. Ladd, F. Jelezko, R. Laflamme, Y. Nakamura, C. Monroe, and J. L. O'Brien, "Quantum computers," Nature **464**, 45–53 (2010).
10. R. van Meter, T. D. Ladd, A. G. Fowler, and Y. Yamamoto, "Distributed quantum computation architecture using semiconductor nanophotonics," Int. J. Quantum. Inform. **08**, 295–323 (2010).
11. T. Yoshie, A. Scherer, J. Hendrickson, G. Khitrova, H. M. Gibbs, G. Rupper, C. Ell, O. B. Shchekin, and D. G. Deppe, "Vacuum Rabi splitting with a single quantum dot in a photonic crystal nanocavity," Nature **432**, 200–203 (2004).
12. T. G. Tiecke, J. D. Thompson, N. P. de Leon, L. R. Liu, V. Vuletic, and M. D. Lukin, "Nanophotonic quantum phase switch with a single atom," Nature **508**, 241–244 (2014).
13. H.-J. Briegel, W. Dür, J. I. Cirac, and P. Zoller, "Quantum repeaters: the role of imperfect local operations in quantum communication," Phys. Rev. Lett. **81**, 5932–5935 (1998).
14. J. D. Cohen, S. M. Meenehan, and O. Painter, "Optical coupling to nanoscale optomechanical cavities for near quantum-limited motion transduction," Opt. Express **21**, 11227–11236 (2013).
15. S. Gröblacher, J. T. Hill, A. H. Safavi-Naeini, J. Chan, and O. Painter, "Highly efficient coupling from an optical fiber to a nanoscale silicon optomechanical cavity," Appl. Phys. Lett. **103**, 181104 (2013).
16. J. D. Thompson, T. G. Tiecke, N. P. de Leon, J. Feist, A. V. Akimov, M. Gullans, A. S. Zibrov, V. Vuletic, and M. D. Lukin, "Coupling a single trapped atom to a nanoscale optical cavity," Science **340**, 1202–1205 (2013).
17. A. Snyder and J. Love, *Optical Waveguide Theory* (Springer, 1983).
18. J. D. Love, W. M. Henry, W. Stewart, R. J. Black, S. Lacroix, and F. Gonthier, "Tapered single-mode fibres and devices. I. Adiabaticity criteria," IEE Proceedings J, Optoelectronics (1985-1993) / IEE Proc-J: Optoelectronics **138**, 343–354 (1991).
19. J. E. Hoffman, S. Ravets, J. A. Grover, P. Solano, P. R. Kordell, J. D. Wong-Campos, L. A. Orozco, and S. L. Rolston, "Ultrahigh transmission optical nanofibers," arXiv:1405.3258 (2014).
20. A. Stiebeiner, R. Garcia-Fernandez, and A. Rauschenbeutel, "Design and optimization of broadband tapered optical fibers with a nanofiber waist," Opt. Express **18**, 22677–22685 (2010).

21. S. G. Johnson and J. D. Joannopoulos, "Block-iterative frequency-domain methods for Maxwell's equations in a planewave basis," Opt. Express **8**, 173–190 (2001).
22. L. Tong, R. R. Gattass, J. B. Ashcom, S. He, J. Lou, M. Shen, I. Maxwell, and E. Mazur, "Subwavelength-diameter silica wires for low-loss optical wave guiding," Nature **426**, 816–819 (2003).
23. J. M. Ward, A. Maimaiti, V. H. Le, and S. N. Chormaic, "Optical micro- and nanofiber pulling rig," arXiv:1402.6396 (2014).
24. G. Brambilla, "Optical fibre nanowires and microwires: a review," J. Opt. **12**, 043001 2010.
25. B. Wang and L.-M. Duan, "Engineering superpositions of coherent states in coherent optical pulses through cavity-assisted interaction," Phys. Rev. A **72**, 022320 (2005).
26. G. Shambat, S.-R. Kothapalli, J. Provine, T. Sarmiento, J. Harris, S. S. Gambhir, and J. Vucković, "Single-cell photonic nanocavity probes," Nano Lett. **13**, 4999–5005 (2013).